CARBON 77 (2014) 390–397

Available at www.sciencedirect.com

ScienceDirect

journal homepage: www.elsevier.com/locate/carbon

Interfacial shear strength of reduced graphene oxide polymer composites

Hong-Kyu Jang [a,b], Hyung-Ick Kim [b,c], Thomas Dodge [d], Pengzhan Sun [e], Hongwei Zhu [e], Jae-Do Nam [f], Jonghwan Suhr [f,*]

[a] Composites Research Center, Korea Institute of Materials Science, Changwon 642-831, South Korea
[b] Center for Composite Materials, University of Delaware, Newark, DE 19716, USA
[c] Manufacturing Process Technology Innovation Center, Korean Institute of Industrial Technology, Jinju 660-805, South Korea
[d] Department of Mechanical Engineering, University of Delaware, Newark, DE 19716, USA
[e] School of Materials Science and Engineering, Tsinghua University, Beijing 100084, China
[f] Department of Polymer Science & Engineering, Department of Energy Science, Sungkyunkwan University, Suwon 440-746, South Korea

ARTICLE INFO

Article history:
Received 11 January 2014
Accepted 17 May 2014
Available online 24 May 2014

ABSTRACT

Interfacial shear strength (IFSS) between particle and matrix in particulate polymer composites is a critical property in determining the mechanical behaviors since it is directly related to not only their Young's modulus or specific strength, but also energy absorbing capability. However, the conventional techniques often present a technical challenge to accurately measure the IFSS between fillers and matrix in the composites. This is more apparent in graphene particulate composites due to their nano-scale dimensions as well as the platelet-shaped geometry. Here, the focus of this study is to use a semi-empirical approach to determine the IFSS of graphene particulate composites by combining experiments with finite element (FE) modeling. The materials of interest are reduced graphene oxide (RGO) and polycarbonate (PC). The tensile testing was performed to characterize the mechanical properties, while simultaneously monitoring the acoustic emission events in order to measure the global debonding stress (GDS) in the composites. By coupling thermal stress analysis and deformation analysis with the GDS as input to a FE model, the IFSS of the RGO particulate PC composites was successfully estimated by about 136 MPa, avoiding unnecessary assumptions and uncertainties which are seem to be inevitable with the conventional techniques for the IFSS measurement.

1. Introduction

Very recently graphene based polymer composites have been extensively studied in order to improve electrical and mechanical properties of a polymer. The extraordinary electrical and mechanical properties of the graphene along with their high specific surface area suggest the use of them in a variety of engineering applications [1–3]. However, the synthesis of pristine graphene is quite expensive and involved in complicated processing, which yet leads to small yield. Attention has been paid to reduced graphene oxide (RGO) that has a very similar structure but higher electrical conductivity when compared to graphene oxide (GO). The RGO can be readily produced in bulk quantity via a chemical

* Corresponding author.
E-mail address: suhr@skku.edu (J. Suhr).
http://dx.doi.org/10.1016/j.carbon.2014.05.042
0008-6223/

and thermal reduction treatment from the GO, which can be synthesized by mechanical cleavage and liquid phase exfoliation of the bulk graphite [2–4]. Therefore, in addition to the electrical conductivity, the RGO has been studied for the use as reinforcement in a polymer composite for improving mechanical properties including Young's modulus, tensile strength, and toughness over neat polymer [4–7].

It is well-known that the mechanical properties of particulate polymer composites are dominated mainly by dispersion, alignment, and interfacial properties of the particles. In particular, the interfacial properties between particles and matrix are known to be critically important in determining the mechanical properties of the composites. For instance, debonding at the interface between the particle and the matrix is directly related to load transfer efficiency and energy absorbing capability in the particulate composites [8,9]. A number of literatures on the studies of the improvement in the mechanical properties of graphene or carbon nanotubes based nanocomposites are available. Platelet-shaped RGO particles have higher specific surface area when compared to carbon nanotubes at the equivalent volume fractions [10]. Based on geometry calculation, platelet-shaped RGO is shown to have almost up to twice greater surface area over single-walled carbon nanotubes (SWCNT). The higher specific surface area allows for more chance for physical interactions and adhesions between the particle and the matrix [6]. As a result, the RGO platelet could be used to more efficiently tailor the ultimate mechanical properties of the composites over the SWCNT or multi-walled carbon nanotubes (MWCNT) based composites. For the RGO particulate composites, it will be important to determine the debonding stress at the interface between RGO platelet and matrix in analysis and design of such particulate nanocomposites. It is not unusual that for a particulate composite, the debonding occurs when the maximum interfacial shear stress in the vicinity of the particle reaches the interfacial shear strength (IFSS). The corresponding stress value, IFSS, is considered to be local debonding stress (LDS) in such a particulate composite [11].

Considerable effort has been made to directly and indirectly measure the IFSS of particulate composites. There are a couple of conventional techniques such as microindentation, microdroplet, and fragmentation methods for the direct determination of the IFSS between particle and matrix. However, the reported IFSS values in the MWCNT reinforced composites present a pretty wide range from 3.5 to 380 MPa [12–15]. Gong et al. [16] and Young et al. [17] observed the stress-induced Raman band shift of the monolayer graphene composites to indirectly measure the IFSS of graphene and they found the value is to be ~2 MPa. In contrast, computational modeling using molecular dynamics (MD) simulations has been used to calculate the interfacial properties of the graphene in polymer composite and the predicted IFSS values are in the range 100–140 MPa [18,19]. The literature survey indicates that although the composites have similar materials for the constituents, the IFSS values are shown to have a large scatter, however. In addition to the technical difficulties in the measurement, the dependence of the IFSS values on each specific experiment configuration along with uncertainties and/or assumptions would be attributed to the inevitably significant scatter. This will be particularly true in determining the IFSS in platelet-shaped graphene based particulate composites due to their geometry as well as the nano-scale dimensions.

In order to address the aforementioned issue, this study employs a semi-empirical approach to effectively and accurately determine the IFSS of graphene particulate polymer composites. The materials of interest in this study are reduced graphene oxide (RGO) and polycarbonate (PC) as nano-scale fillers and matrix, respectively. The RGO platelets were synthesized via a thermal reduction treatment, and the RGO particulate PC composites were fabricated by using a solution mixing technique. The tensile testing was performed to characterize the mechanical properties of the composites, simultaneously monitoring the acoustic emission (AE) events in order to measure the averaged debonding stress, which can be defined as the global debonding stress (GDS) of the composites. Thermal stress finite element (FE) analysis was first performed for taking into account the thermal residual stress in the vicinity of the RGO particle in the composite, which was then coupled by deformation analysis with the GDS as input to a micromechanics based FE model of representative volume element (RVE). This study demonstrates that the IFSS of the platelet-shaped RGO particulate PC composites was successfully estimated by about 136 MPa via the semi-empirical approach. Encouragingly, others also reported similar results with the molecular dynamic simulation on the IFSS in between graphene and a polymer.

2. Experimental

2.1. Synthesis of reduced graphene oxide

GO sheets were prepared by a modified Hummers' method using worm-like graphite as the source according to our previous work [20,21]. Natural graphite flakes were mixed with hydrogen peroxide and concentrated sulfuric acid, stirred, washed, and dried. The resultant graphite intercalation compounds were fast heated at 900 °C for 10 s to gain the expanded worm-like graphite flakes. Then the worm-like graphite flakes were transformed into GO flakes by the modified Hummers' method using concentrated sulfuric acid, potassium permanganate and sodium nitrite according to an established method [22,23]. Afterwards, the as-prepared GO sheets were thermally reduced at 300 °C for 30 min in an Ar atmosphere and finally the RGO flakes were obtained.

2.2. Fabrication of particulate composites

In order to maintain the good dispersion quality and isolate the effect of the RGO loading fraction, the RGO weight fractions of only up to 0.5% were selected in this study. In addition, to achieve more uniform distribution of the RGO platelets in the PC matrix, a solution mixing method was employed. First, the RGO platelets and PC granules (Goodfellow Corporation) were dehumidified in a vacuum oven (Isotemp Vacuum Oven Model 281A) at 90 °C for 12 h. The dehumidified RGO platelets and PC granules were dispersed and dissolved separately using a probe sonicator (Misonix Ultrasonic Liquid Processor) in tetrahydrofuran (THF) solvent.

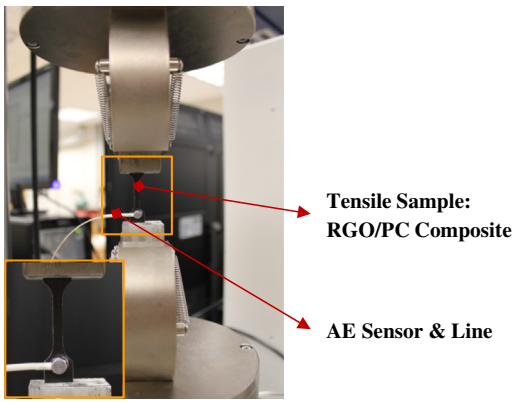

Fig. 1 – Photographic image of the test setup for combined tensile and acoustic emission testing. (A colour version of this figure can be viewed online.)

The two solutions were mixed with the desirable weight fractions of the RGO platelet (0.15, 0.25, 0.35 and 0.50 wt%). The mixtures were sonicated again to get uniformed dispersion in the solution and then poured into methanol solvent to obtain the precipitated RGO/PC composite materials. In order to obtain the RGO/PC composite powder, the precipitate was filtered using a filtration pump (KNF Neuberger, Inc.) and dried out to remove any remaining solvent at 90 °C for 24 h in a vacuum oven. The dog-bone shaped tensile specimens were fabricated using a compressive mold, which was preheated at 180 °C. The dimensions of the tensile specimens are 3.2 mm in width, 0.8 mm in thickness, and 63.5 mm in length (ASTMD 638 Type V). Fig. 3d shows the scanning electron microscope (SEM) image (Jeol JSM-7400F) of the sonicated RGO platelets in THF solvent prior to adding into the matrix material. More details on the composite fabrication process can be found elsewhere [24,25].

2.3. *Tensile test and acoustic emission test*

The tensile testing for all composite samples (neat, 0.15, 0.25, 0.35, and 0.50 wt%) was conducted by using ElectroPlus E3000 (Instron Corporation) for characterizing the Young's modulus, the tensile strength and the toughness. A crosshead speed of 10 mm/min according to ASTM D638, and a 3 kN load cell were chosen for the characterization. During the tensile testing, the AE signals were monitored in order to identify the debonding failure mode in the composites. The AE acquisition system was set up in a single sensor mode with a transducer (Physical Acoustics Corporation) and the signals were counted in a time interval of 0.01 s with respect to the applied stress [26]. The experiment setup for the combined tensile and AE testing is seen in Fig. 1.

3. Finite element modeling

A FE model of RVE for the RGO particulate PC composites was developed in order to estimate local debonding stress between RGO platelets and PC matrix (Supplementary Data: S1). The detailed physical properties for the FE model of RVE are listed in the Table 1 [27,28]. For more accurate prediction, the effective Young's modulus of the RGO platelet was calculated by around 305 GPa for the FE analysis (Supplementary Data: S2). The developed FE model of RVE was seen in Fig. 2 showing the FE meshes, loading, and boundary conditions. An 8 node three dimensional linear brick element (C3D8R) of commercial software ABAQUS 6.11 was used for the both RGO platelet and PC matrix modeling. In this study, we created a half FE model with the z-axis symmetric boundary condition ($z = 0$ plane) taking advantage of the geometric symmetry. In addition, the left surface of the FE model ($x = 0$ plane) was fixed against movement along the X direction and the displacement constraints for the RVE boundary were imposed on the other three surfaces.

4. Results and discussion

4.1. *Morphology and characterization of RGO*

Fig. 3a shows the SEM characterization of the synthesized RGO flakes, which reveals that the as-prepared GO flakes have the lateral size of several hundred nanometers to several micrometers. For the GO flakes, a large amount of oxygen-containing functional groups were decorated on the basal planes and the edges as shown in Fig. 3b. The oxygen percentage within the as-prepared GO flakes was found to be about 32.5%. After thermal reduction treatment at 300 °C for 30 min, the GO sheets were transformed to the RGO flakes and most of the oxygen-containing functional groups were removed from the GO sheet as seen in the XPS analysis results (Fig. 3c). According to the XPS results, the oxygen percentage on the GO sheets was reduced down to about 15.5%, which is an indicative of an efficient reduction of the GO sheets via the thermal treatment.

4.2. *Tensile properties of RGO polymer composites*

RGO particulate PC composites were fabricated by using a solution mixing technique and then tensile testing was performed to characterize the tensile properties of the composites. The tensile properties such as the Young's modulus and tensile strength are compared by varying the RGO loading

Table 1 – Geometrical information and physical properties of the RVE model for 0.5 wt% RGO particulate PC composites.

	Young's modulus (GPa)	Tensile strength (MPa)	Poisson ratio	Density (g/cm^{-3})	Thermal expansion ($10^{-6}/K$)	Width & length (μm)	Thickness (μm)
RGO	305	>120	0.17	1.80	−2	30	0.2
PC	1.80	66	0.37	1.20	68.4	37.777	37.777

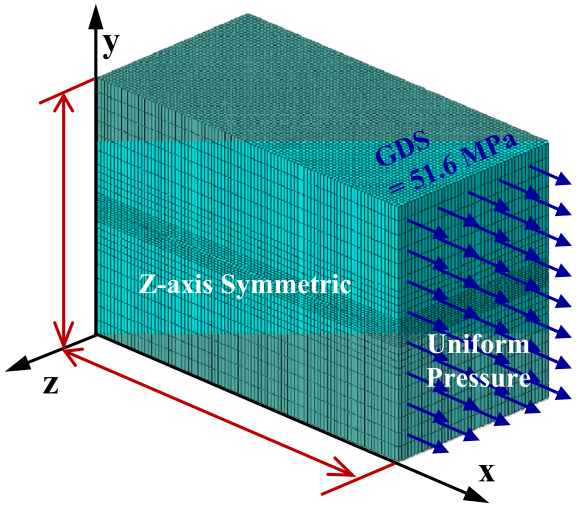

Fig. 2 – A half finite element (FE) model of representative volume element (RVE) for the RGO reinforced PC composite showing fine mesh on RGO and the loading and boundary conditions. (A colour version of this figure can be viewed online.)

fractions (0.15, 0.25, 0.35, and 0.50 wt%) as seen in Fig. 4a and b. It was seen in Fig. 4a that the greatest improvement in the Young's modulus for the RGO composites was measured by only 10% enhancement over the neat PC. It can be expected that the reinforcement effect might be insignificant in the composites with the addition of such low RGO loading fractions. Interestingly, the tensile strength at each the RGO loading fraction was found to be more or less the same value of the neat PC, indicating no enhancement in tensile strength of the polymer (Fig. 4b). Also, note that the tensile toughness behavior of the composites was shown to be similar to the tensile strength behavior (not seen in this paper).

Statistical analyses on the tensile data were further conducted by the use of liner curve fitting in conjunction with analysis of variance (ANOVA) test. The statistical analysis results are summarized in Table S1 (Supplementary Data: S3), and seen in Fig. 4c and d. The results can confirm that the Young's modulus behavior of the RGO particulate composites exhibits a moderate increase with the increase in the RGO loading fractions (Fig. 4c), while no significant difference in the tensile strength is found over the loading fractions investigated in this study (Fig. 4d). It is noted that these results seem to be consistent with the others [7,29,30].

4.3. *Debonding stress of RGO polymer composites*

It is necessary to experimentally measure the GDS of the RGO composites to be used as input to the FE model for estimation of the LDS between the RGO platelet and the PC, which is discussed later. The AE test was simultaneously performed during the tensile testing in order to detect the identify failures including matrix breaks and particle debonding in the particulate composites. By monitoring the maximum number of the AE events and then taking the corresponding tensile stress value, the GDS of the RGO particulate composites was

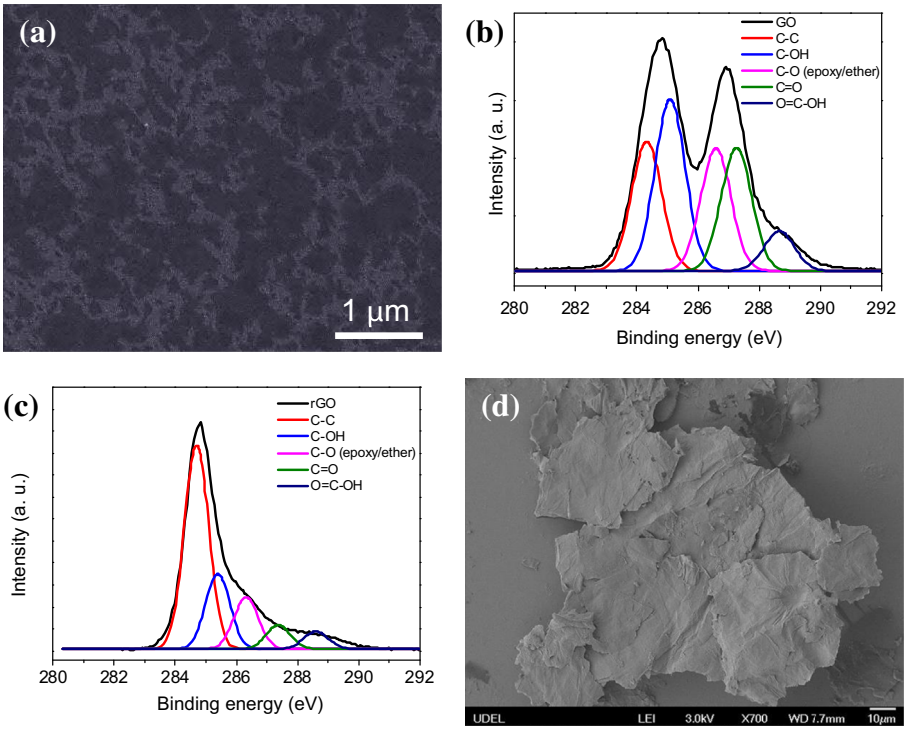

Fig. 3 – Characterization of reduced graphene oxide. (a) SEM image of the as-prepared RGO flakes, (b) XPS analysis of the GO sheets, (c) XPS analysis of the RGO flakes, and (d) SEM image of the RGO platelets after sonication. (A colour version of this figure can be viewed online.)

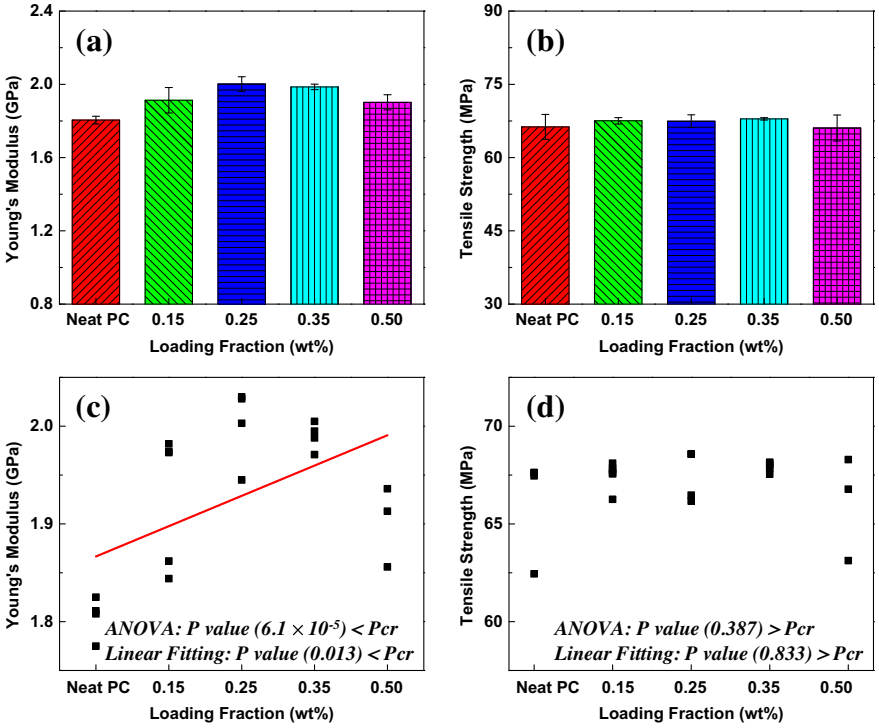

Fig. 4 – Characterization of tensile properties of neat PC and RGO particulate PC composites. (a) Young's modulus of neat PC and RGO/PC composites, (b) tensile strength of neat PC and RGO/PC composites, (c) statistical analysis on the Young's modulus (a linear dependence with respect to the loading fraction is seen), and (d) statistical analysis on the tensile strength (no dependence between tensile strength and loading fractions). (A colour version of this figure can be viewed online.)

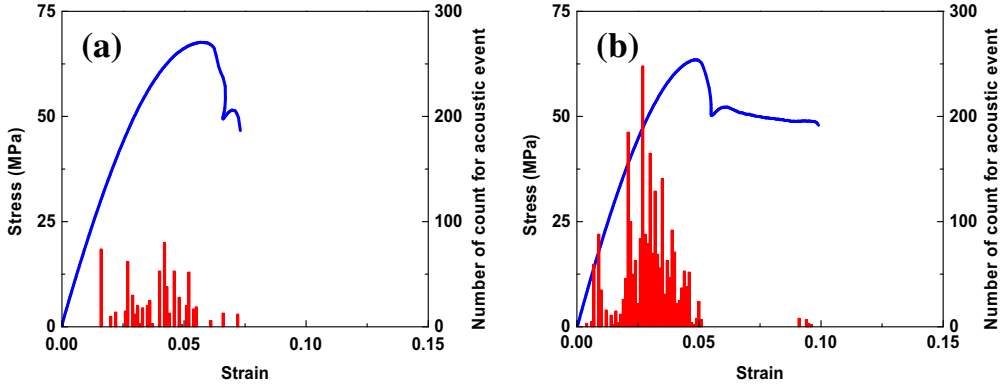

Fig. 5 – Stress–strain curves and the corresponding number of acoustic emission (AE) events. (a) Neat PC composite and (b) 0.5 wt% RGO particulate PC composite. (A colour version of this figure can be viewed online.)

analyzed and determined [31]. Fig. 5a and b show the stress–strain curves and the corresponding AE events of a representative sample of neat PC and 0.5 wt% of RGO reinforced PC composites, respectively. According to the AE test results (Fig. 5), the 0.5 wt% RGO composite showed a normal distribution and the maximum number of the events were around 250 at the stress level of about 48.7 MPa (Fig. 5b), which would be the GDS in the composite. In contrast, whereas far less number of the AE events were recorded for the neat PC over the corresponding stress level. As expected, the more AE events are counted from the RGO particulate composites over the neat PC. This is because while the RGO composites would generate the AE events from not only the matrix failures but also the debonding between the RGO and the PC matrix when compared to the neat PC which will have only matrix material failures during tensile testing. It is seen in Fig. 6a that the GDS values were measured by from 49.4 to 54.3 MPa over the four different RGO loading fractions (5 test samples for each loading fraction: 0.15, 0.25, 0.35, and 0.50 wt%). However, the statistical analysis indicates that there is no significant difference between the obtained GDS values (Fig. 6b). For the consequence and convenience, we take the averaged value of 51.6 MPa as the GDS in the RGO particulate PC composites.

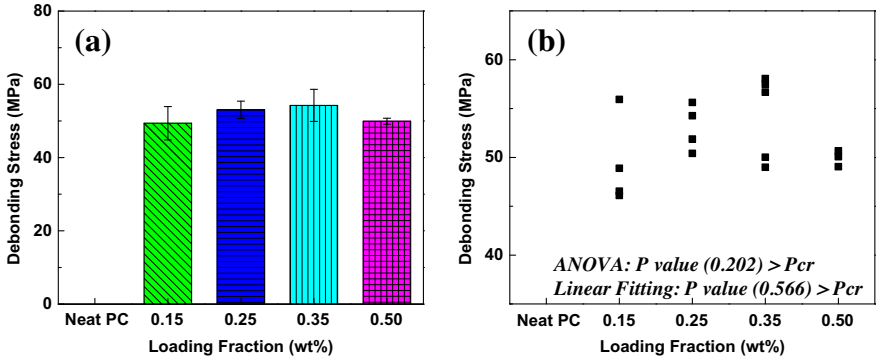

Fig. 6 – (a) Global debonding stress of RGO particulate PC composites and (b) statistical analysis on the debonding stress data with respect to the RGO loading fractions. (A colour version of this figure can be viewed online.)

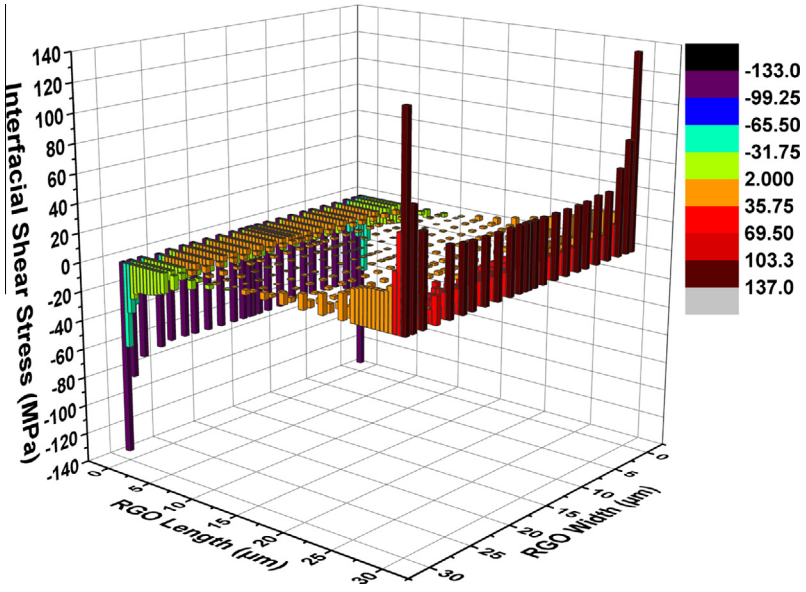

Fig. 7 – Estimated interfacial shear stress values along the square RGO platelet (30 μm × 30 μm) in the particulate polymer composites. (A colour version of this figure can be viewed online.)

4.4. *Interfacial shear strength of RGO polymer composites*

Prior to the deformation analysis, thermal stress analysis was performed to account for the thermal residual stress that is developed in the vicinity of the RGO platelet during the composite manufacturing process before application of any external loads. Given that sufficiently accurate estimation of the IFSS (or LDS) of the composites is essential in this study, the thermal stress analysis was first conducted to simulate the annealing process during the composite fabrication by imposing the temperature change from 180 °C to room temperature. Afterwards, the structural stress analysis was coupled by applying the uniaxial load described above; where the imposed stress was equal to the experimentally measured GDS (51.6 MPa) in the earlier testing. By superimposing the thermal residual stress into the structural stress at the interface between the RGO and the matrix of the FE model, the more accurate IFSS (or LDS) of the RGO composites is able to be estimated. The calculated structural shear stress distribution contour along the RGO platelet, which results from the coupled thermal residual stress and deformation analysis, is seen in Fig. S2 (Supplementary Data: S4).

Fig. 7 shows the calculated interfacial shear stress values along with the RGO platelet in the RVE FE model (Fig. 7). According to the FE results, the maximum shear stress was found at the each edge of the RGO platelet, which can be readily expected from the Cox-based shear lag model [32]. As aforementioned, the maximum shear stress in the vicinity of the particle is assumed to be the LDS, which will be then equal to the IFSS of the RGO platelet in the particulate composites. In this way, the IFSS was successfully evaluated by around 136 MPa via the semi-empirical approach taken in this study. Similar results on the IFSS ranging from 106 to 141 MPa between three layer graphene sheets and vinyl ester matrix were reported by others based on MD simulation, which is encouraging [19].

5. Conclusion

In this study, a semi-empirical approach was successfully demonstrated by combining experiments and FE modeling, which allows for the determination of the IFSS of RGO platelet in the RGO particulate polycarbonate composites. The RGO particulate composites were fabricated via a solution mixing method and their tensile properties were characterized by varying the RGO loading fraction. The AE events were simultaneously monitored during the tensile testing. It was experimentally observed that the Young's modulus of the composites was slightly increased as the RGO loading fraction increases up to 0.5 wt%. In addition, from the coupled tensile test and AE technique, the GDS of the RGO composites was measured in order to be used as input to the FE model of RVE for the particulate composites. After that, the coupled FE analysis was conducted by accounting for the thermal residual stress and structural stress. By the use of the semi-empirical approach, the IFSS between the RGO platelet and the PC in the nanocomposites was evaluated and estimated by about 136 MPa. This allows for avoiding unnecessary assumptions and uncertainties, which seem to be inevitable with the conventional techniques for the IFSS measurement. To the best of our knowledge, this is the first experimental study to determine the IFSS between graphene based fillers and polymer matrix in nanocomposites. We believe that this is an important contribution for better understanding and designing on the composites particularly with nano-scale reinforcements such as graphene or carbon nanotubes for various engineering structural applications.

Acknowledgments

This work was supported by the WPM (World Premier Materials) Program, Project No. 10037878, Utralight Structural Nano Carbon Composite, funded by the Ministry of Trade, Industry & Energy (MI, South Korea). The authors also acknowledge the financial support from the National Science Foundation, Award No. 1104640 (United States).

Appendix A. Supplementary data

Supplementary data associated with this article can be found, in the online version, at http://dx.doi.org/10.1016/j.carbon.2014.05.042.

REFERENCES

[1] Young RJ, Kinloch IA, Gong L, Novoselov KS. The mechanics of graphene nanocomposites: a review. Compos Sci Technol 2012;72(12):1459–76.
[2] Zhu Y, Murali S, Cai W, Li X, Suk JW, Potts JR, et al. Graphene and graphene oxide: synthesis, properties, and applications. Adv Mater 2010;22(35):3906–24.
[3] Verdejo R, Bernal MM, Romasanta LJ, Lopez-Manchado MA. Graphene filled polymer nanocomposites. J Mater Chem 2011;21:3301–10.
[4] Kuilla T, Bhadra S, Yao D, Kim NH, Bose S, Lee JH. Recent advances in graphene based polymer composites. Prog Polym Sci 2010;35(11):1350–75.
[5] Kim HW, Abdala AA, Macosko CW. Graphene/polymer nanocomposites. Macromolecules 2010;43(16):6515–30.
[6] Rafiee MA, Rafiee J, Wang Z, Song H, Yu ZZ, Koratkar NA. Enhanced mechanical properties of nanocomposites at low graphene content. ACS Nano 2009;3(12):3884–90.
[7] Rafiee MA, Rafiee J, Srivastava I, Wang Z, Song H, Yu ZZ, et al. Fracture and fatigue in graphene nanocomposites. Small 2010;6(2):179–83.
[8] Sun L, Gibson RF, Gordaninejad F, Suhr J. Energy absorption capability of nanocomposites: a review. Compos Sci Technol 2009;69(14):2392–409.
[9] Fu S, Feng X, Lauke B, Mai Y. Effects of particle size, particle/matrix interface adhesion and particle loading on mechanical properties of particulate–polymer composites. Compos B: Eng 2008;39(6):933–61.
[10] Ma PC, Siddiqui NA, Marom G, Kim JK. Dispersion and functionalization of carbon nanotubes for polymer-based nanocomposites: a review. Compos A: Appl S 2010;41(10):1345–67.
[11] Hsueh CH, Becher PF. Interfacial shear debonding problems in fiber-reinforced ceramic composites. Acta Mater 1998;46(9):3237–45.
[12] Cooper CA, Cohen SR, Barber AH, Wagner HD. Detachment of nanotubes from a polymer matrix. Appl Phys Lett 2002;81(20):3873–5.
[13] Tsuda T, Ogasawara T, Deng F, Takeda N. Direct measurements of interfacial shear strength of multi-walled carbon nanotube/PEEK composite using a nano-pullout method. Compos Sci Technol 2011;71(10):1295–300.
[14] Zu M, Li Q, Zhu Y, Dey M, Wang G, Lu W, et al. The effective interfacial shear strength of carbon nanotube fibers in an epoxy matrix characterized by a microdroplet test. Carbon 2012;50(3):1271–9.
[15] Liu YN, Li M, Gu Y, Zhang X, Zhao J, Li Q, et al. The interfacial strength and fracture characteristics of ethanol and polymer modified carbon nanotube fibers in their epoxy composites. Carbon 2013;52:550–8.
[16] Gong L, Kinloch LA, Young RJ, Riaz L, Jalil R, Novoselov KS. Interfacial stress transfer in a graphene monolayer nanocomposite. Adv Mater 2010;22:2694–7.
[17] Young RJ, Gong L, Kinloch LA, Riaz L, Jalil R, Novoselov KS. Strain mapping in a graphene monolayer nanocomposite. ACS Nano 2011;5:3079–84.
[18] Awasthi AP, Lagoudas DC, Hammerand DC. Modeling of graphene-polymer interfacial mechanical behavior using molecular dynamics. Model Simul Mater Sci Eng 2009;17:015002.
[19] Jang C, Lacy TE, Gwaltney SR, Toghiani H, Pittman Jr CU. Interfacial shear strength of cured vinyl ester resin-graphite nanoplatelet from molecular dynamics simulations. Polymer 2013;54(13):3282–9.
[20] Gu W, Zhang W, Li X, Zhu H, Wei J, Li Z, et al. Graphene sheets from worm-like exfoliated graphite. J Mater Chem 2009;19:3367–9.
[21] Sun P, Zhu M, Ma R, Wang K, Wei J, Wu D, et al. Graphene oxide/titania hybrid films with dual-UV-responsive surfaces of tunable wettability. RCS Adv 2012;2(29):10829–35.
[22] Stankovich S, Dikin DA, Piner RD, Kohlhaas KA, Kleinhammes A, Jia Y, et al. Synthesis of graphene-based nanosheets via chemical reduction of exfoliated graphite oxide. Carbon 2007;45(7):1558–65.
[23] Eda G, Fanchini G, Chhowalla M. Large-area ultrathin films of reduced graphene oxide as a transparent and flexible electronic material. Nat Nanotechnol 2008;3:270–4.

[24] Koratkar NA, Suhr J, Joshi A, Kane RS, Schadler LS, Ajayan PM, et al. Characterizing energy dissipation in single-walled carbon nanotube polycarbonate composites. Appl Phys Lett 2005;87(6):063102.
[25] Suhr J, Zhang W, Ajayan PM, Koratkar NA. Temperature-activated interfacial friction damping in carbon nanotube polymer composites. Nano Lett 2006;6(2):219–23.
[26] Cho MR, Kim HI, Jang JS, Suhr J, Prate DR, Chun D. Investigation of mechanical damping characteristic in short Fiberglass reinforced polycarbonate composites. Mod Phys Lett B 2013;27(15):1350108.
[27] Yoon D, Son YW, Cheong H. Negative thermal expansion coefficient of graphene measured by Raman spectroscopy. Nano Lett 2011;11(8):3227–31.
[28] Dikin DA, Stankovich S, Zimney EJ, Piner RD, Dommett GHB, Evmenenko G. Preparation and characterization of graphene oxide paper. Nature 2007;448:457–60.
[29] Tang LC, Wan YJ, Yan D, Pei YB, Zhao L, Li YB, et al. The effect of graphene dispersion on the mechanical properties of graphene/epoxy composites. Carbon 2013;60:16–27.
[30] Guo J, Liu Y, Prada-Silvy R, Tan Y, Azad S, Krause B, et al. Aspect ratio effects of multi-walled carbon nanotubes on electrical, mechanical, and thermal properties of polycarbonate/MWCNT composites. J Polym Sci B: Polym Phys 2014;52(1):73–83.
[31] Minko S, Karl A, Voronov A, Senkovskij V, Pomper T, Wilke W, et al. Evaluation of the polymer–nanopolymer adhesion in particle-filled polymers with the acoustic emission method. J Adhes Sci Technol 2000;14(8):999–1019.
[32] Gibson RF. Principles of composite material mechanics. 3rd ed. Boca Raton: CRC Press; 2012. 219–282.